JTTEE5 15:773-778
DOI: 10.1361/105996306X146730
1059-9630/$19.00 © ASM International

Ambient and High-Temperature Thermal Conductivity of Thermal Sprayed Coatings

W. Chi, S. Sampath, and H. Wang

(Submitted April 3, 2006; in revised form July 13, 2006)

Aside from its importance as a design parameter for thermal barrier coatings, measuring thermal conductivity of thermal sprayed coatings itself provides a unique method to critically characterize the nature, quantity, and anisotropy of the defect morphologies in these splat-based coatings. In this paper, the authors present a systematic assessment of thermal conductivity of wide range using the flash diffusivity technique. For the case of plasma sprayed yttria-stabilized zirconia (YSZ), coatings obtained from wide-ranging initial powder morphologies as well as those fabricated under different particle states were characterized. Both in-plane and through-thickness properties were obtained. Other material systems that were considered include: metallic alloys and semiconductors of interests. Issues such as reproducibility and reliability in measurements were also considered and assessed. Finally, work in collaboration with the Oak Ridge National Laboratory (ORNL) for alternate approaches to characterization of thermal conductivity as well as high-temperature measurements was performed.

Keywords porosity of coatings, thermal barrier coatings, thermal properties

1. Introduction

Thermal barrier coatings (TBC) are designed to protect the components from harsh and severe thermal environments (Ref 1). The remarkable feature of the TBC is its survivability, both in thermal shock and in the difficult environmental conditions within the gas turbine and diesel engines (Ref 2). For plasma sprayed TBCs, control of thermal conductivity is critical since low thermal conductivity depends not only on the intrinsic property of coatings, but also on the morphology of pores and cracks introduced during spray process (Ref 3). Thermal energy is transported in solid insulating materials mainly by phonons at ambient temperature. Thermal conductivities of these materials are temperature and chemical composition dependent (Ref 4, 5). The thermal sprayed coating has lower thermal conductivity than the bulk material with the same composition due to the contribution of microstructural features (pores, cracks, etc.). Thus, it is necessary to understand and describe the relationship between the thermal conductivity and defects both at ambient and, in the case of TBC, at operation temperature. The microstructure of plasma sprayed coatings has been modeled as regions of perfect contact between lamellas separated by very thin regions of no contact arising from gas entrapped by spreading liquid droplets during coating formation (Ref 6). The very low thermal conductivity of the coatings can be partially justified by noncontact regions having low thermal conductance, since their thickness is comparable to the mean free path of the gas molecules within them (Ref 7, 8).

This paper examines the thermal conductivity as it relates to the microstructure and its dependent factors, such as particle state, measurement temperature, and chemical components. Of principle interest is the relation of the critical role of microstructural defects to the reduction in thermal conductivity for various sprayed coatings. Anisotropic thermal conductivity of the TBC is also investigated and correlated with anisotropy of microstructure. Finally, the results of thermal conductivity measured by different techniques are compared and elucidated.

2. Experimental

Three morphology YSZ powders were used as the materials of ceramic coatings nominally with the same size distribution: hollow sphere (HOSP, 27 to 95 μm, d_{50} = 60 μm), agglomerated and sintered (A&S, 27 to 97 μm, d_{50} = 55 μm), and fused and crushed (F&C, 31 to 97 μm, d_{50} = 64 μm). Molybdenum (Mo) (55 to 77 μm, d_{50} = 63 μm) powders were also adopted to make metal coatings. All the aforementioned coatings were deposited by Sulzer Metco APS 7MB (Sulzer Metco, Winterthur, Switzerland) torch with an 8 mm nozzle. The processing parameters are shown in Table 1.

Table 1 Processing parameters of ceramic and metal coatings

Spray torch	HOSP	A&S	F&C	Mo
Secondary gas H_2, slpm	6.9	6.9	6.9	3.0
Primary gas N_2, slpm	51.9	51.7	45.3	38.3
Carrier gas N_2, slpm	4.13	5.97	4.81	2.2
Current, A	513	548	675	500
Voltage, V	79.3	76.1	73	64
Standoff, mm	130	130	130	100
Feed rate, g/min	20	20	30	40

This article was originally published in *Building on 100 Years of Success, Proceedings of the 2006 International Thermal Spray Conference* (Seattle, WA), May 15-18, 2006, B.R. Marple, M.M. Hyland, Y.-Ch. Lau, R.S. Lima, and J. Voyer, Ed., ASM International, Materials Park, OH, 2006.

W. Chi and **S. Sampath,** Center for Thermal Spray Research, State University of New York, Stony Brook, NY; and **H. Wang,** High Temperature Materials Laboratory, Oak Ridge National Laboratory, Oak Ridge, TN. Contact e-mail: wchi@ic.sunysb.edu.

Table 2 Processing parameters of semiconductor coating

Material	Secondary gas H_2, slpm	Primary gas Ar, slpm	Carrier gas Ar, slpm	Current, A	Voltage, V	Standoff, mm	Feed rate, g/min
Si	10	50	5	500	68	100	15

Also, a semiconductor coating was successfully deposited using silicon (Si) powder (2 to 40 μm, d_{50} = 12 μm) and a plasma gun Sulzer Metco F4MB with a 6 mm nozzle. Table 2 lists the torch parameters of Si coating.

In addition, F&C powder was selected to make coatings at different temperature and velocity for the study of particle state effect. The details are discussed in the section related to process map.

Thermal conductivity measurements were carried out on disk-shaped specimens, coated with graphite. Three kinds of flash diffusivity techniques were used to measure ambient or high-temperature thermal conductivity of thermal sprayed coatings.

2.1 Xenon Flash Thermal Diffusivity (XFTD) System

Reliable measurement of thermal diffusivity in many cases can be obtained through the xenon flash technique. The xenon flash thermal diffusivity system is optimized for room-temperature thermal diffusivity measurements of ceramics, metals, composites, and coatings. However, this system cannot be used to measure thermal conductivity directly. A separate differential scanning calorimeter (DSC) system is necessary to measure heat capacity (C_p) to calculate thermal conductivity, and its accuracy is about 1 to 2% (Ref 9). The formula for thermal conductivity calculation is $K = \alpha\rho C_p$, where K is the thermal conductivity, ρ is the bulk density, and C_p is the specific heat. The accuracy of XFTD is somewhat better than that of laser flash instrument due to the short detector-to-sample distance and low signal-to-noise ratio.

2.2 Laser Flash Instrument for Room Temperature (RT)

Microflash instrumentation can be used to measure both thermal diffusivity and thermal conductivity by obtaining C_p and α in one test. In the through-thickness measurement, the sample can be thought of as part of a sheet of material infinite in two dimensions but of finite thickness. A test sample is irradiated uniformly on one side using a single laser beam pulse. The measurement of the thermal diffusivity of a material is usually carried out by rapidly heating one side of a sample and measuring the temperature rise curve on the opposite side. The temperature rise of the other side is measured as a function of time using an infrared (IR) detector. Before the flash, the temperature of sample and surroundings is at some uniform temperature that can be taken as zero. Immediately after the flash, the front surface of the sample is at some higher temperature. The heat flux lines are parallel and directed through the sample; there is no heat flow in the plane of the sample. The time taken for the back surface to reach half its maximum temperature ($t_{1/2}$) should be at least three times longer than the length of the laser pulse (0.33 ms) and no longer than 3 s. The other advantage is that in-plane measurements of thermal diffusivity and conductivity are available. The laser beam is collimated or focused on the front face of the sample, and the distance that heat must flow is significantly greater. A mask with a circular pinhole concentric with the beam axis is used to define the viewing radius of the IR detector. The radial, in-plane measurement does not constrain the heat flow to one or even two dimensions. The heat flow has two components: one through the sample and one in the plane of sample. Heat that flows directly through the samples will be blocked by the mask (Ref 10).

Figure 1 shows the reproducibility of this instrument for measuring thermal conductivity at ambient temperature. To determine the measurement accuracy of this instrument, one standard sample and six yttria-stabilized zirconia (YSZ) coating samples were studied. The thermal conductivity of standard sample (pyroceramic disk) was measured nine times. The coefficient of variation was 1.8%. For an experimental plasma sprayed YSZ specimen, nine measurements were made, resulting in a coefficient of variation 5%. From the same coating, six separated specimens were made and nine measurements were taken for each specimen. The coefficient of variation is 8%. From these measurements, the accuracy of Holometrix laser flash thermal property instrument was found of the order 8% for through-thickness measurement.

2.3 Laser Flash Thermal Diffusivity (LFTD) System for High-Temperature (HT)

The high-temperature thermal property can be measured by the Anter Flashline 5000 LFTD system (Anter Corporation, Pittsburgh, PA) that is designed to acquire data automatically from cryogenic temperatures up to 2500 °C. A small disk-shaped specimen is placed in an evacuated tube furnace and oriented with its flat surfaces perpendicular to the furnace axis. A heat pulse (less than 1 ms) is transmitted to the front face of a specimen using a laser flash, and the temperature change of the rear face is measured with an IR detector. Data analysis algorithms interpret the rear face temperature response and provide instrumental and specimen-dependent corrections. The change of thermal diffusivity with temperature can be obtained by this LFTD system (Ref 11).

3. Results and Discussion

This multifaceted approach to thermal conductivity measurement of thermal sprayed coatings was applied to a variety of thermal sprayed coatings. A wide range of YSZ materials comprising coatings produced from various starting morphology and also through the rigorous process maps served as the stating materials. Details of such process map strategies are presented elsewhere (Ref 12-17). In addition, other metallic and semiconductor coatings were also analyzed for thermal transport property.

3.1 Effect of Feedstock Powder Morphology on Thermal Conductivity of YSZ Coatings

Three commercial YSZ powders of different morphologies were adopted to fabricate coatings. The YSZ powders of three

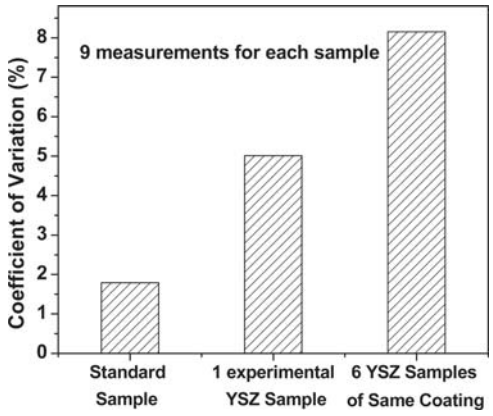

Fig. 1 Fidelity of laser flash thermal conductivity instrument for room temperature

morphologies were obtained from different manufacturing techniques. The fused and crushed (F&C) method involves electric melting of parent ore, solidifying and crushing the ingot, which produces angular/polyhedral particles; the agglomerated and sintered (A&S) technique agglomerates powders with binders and subsequent high-temperature treatment to produce globular/rough-textured particles; and the plasma densified (HOSP) process, involving spray drying and plasma densification, produces hollow sphere powders (Ref 2). All powders nominally have similar particle size distributions conforming to established aeroengine coating specifications. Kulkarni et al. (Ref 2) examined the room-temperature thermal conductivities for YSZ coatings made of different morphology powders (all the materials were deposited using the same process parameters). In the current study, the particle temperature and velocity were optimized for each morphology powder so they all fall nominally at the same average velocity and temperature, referred to as "same *TV*." The average particle temperature and velocity (averaged from 10,000 individual particles using DPV 2000) were achieved as 2661 ± 10 °C and 125 ± 2 m/s respectively. In this way, all the other factors except powder morphology were kept constant, and the effect of powder morphology itself on coating thermal conductivity can be examined.

The cross-section images (Fig. 2) of each sample were taken by Nikon Epiphot 200 optical microscopy (Nikon Corporation, Tokyo, Japan). The thermal conductivity relationship to porosity for YSZ coatings made of different morphology powders is shown in Fig. 3. The results indicate that different morphologies sprayed at nominally the same particle state result in different thermal conductivities. For instance, the A&S powder coating has the highest total porosity, yet its thermal conductivity is higher than that of HOSP deposit. The HOSP coating had almost lowest total porosity and yet lowest thermal conductivity.

These results suggest that pore architecture plays an important role in thermal conductivity. The HOSP material, due to the hollow nature, results in thinner splats and consequently a larger fraction of interlamellar porosity. F&C powder coatings have the highest thermal conductivity due to the lowest total porosity compared with HOSP and A&S powder coatings. As for F&C and A&S powder coatings, although the interlamellar porosity of F&C powder coating is a little higher than that of A&S powder coating, the thermal conductivity of F&C powder coating is higher. This is due to the fact that total porosity of A&S powder coating is much higher and the difference of interlamellar pores between these two coatings is insignificant. The capability of heat impedance of coating microstructural defects is related not only to the pore morphology but also to the amount of different morphology pores.

This explanation can be extended to the case at high temperatures. Figure 4 shows the effect of powder morphology on the temperature-dependent thermal conductivity. The same trend as room-temperature data is observed; the sequence of thermal conductivity from highest to lowest is F&C, A&S, and HOSP powder coatings. The original microstructure and thermal property at room temperature determine the change of thermal conductivity of different morphology powder coatings at high temperatures. The different morphologies of powders result in different porosity and finally thermal conductivity at both room and high temperatures.

Figure 4 shows that thermal conductivity monotonically decreases from room temperature to 800 °C or so because scattering of lattice vibration becomes more pronounced with rising temperature. The shape of the thermal conductivity curves indicates a phonon conduction mechanism up to 800 °C (Ref 4). The thermal conductivity is limited by intrinsic phonon scattering scales as $1/T$ (Ref 18). The thermal conductivities of YSZ coatings made of three different morphology powders begin to increase above 800 °C, which is due to radiant heat transfer. At higher temperatures the photon conduction becomes increasingly important and sintering/densification of the materials begins to occur even during the measurement process (Ref 4). The microstructural defects in the heterogeneous YSZ coating result in the scattering, reflection, and absorption of photons at high temperature. Therefore, the high-temperature thermal conductivity is influenced by pore features, such as porosity, pore size, and pore morphology. Schlichting (Ref 5) et al. examined the correlation of porosity and pore size with thermal conductivity. At first glance, it appears that large pore size increases thermal conductivity. In fact, the increase in pore size results in significant rising of pore volume (porosity), which has a great effect on thermal radiation photon transport. From Fig. 4, the effect of morphology on thermal conductivity is investigated. The coating made by HOSP powder with the large fraction interlamellar porosity has the lowest thermal conductivity. It clearly shows the effect from pore morphology on photon transfer. More quantitative correlations of pore features (porosity, size, distribution, and shape) with thermal radiation photon transport are required to be investigated in the future step.

3.2 Effect of Particle State on Thermal Conductivity YSZ Coating

The particle velocity and temperature control the splat and final coating properties to a great extent. The splat formation is dependent on its melting state and kinetic state and can exhibit a wide range of morphologies—from highly fragmented to contiguous (Ref 13, 19). It is widely appreciated that the variation of velocity and temperature of particles yields different microstructure of YSZ coatings (Ref 20). To explore the effects of particle state on coating microstructure and property, the same F&C YSZ powder was selected to fabricate coatings: R1, R2, R3, and R4. In this method, different process parameters were combined

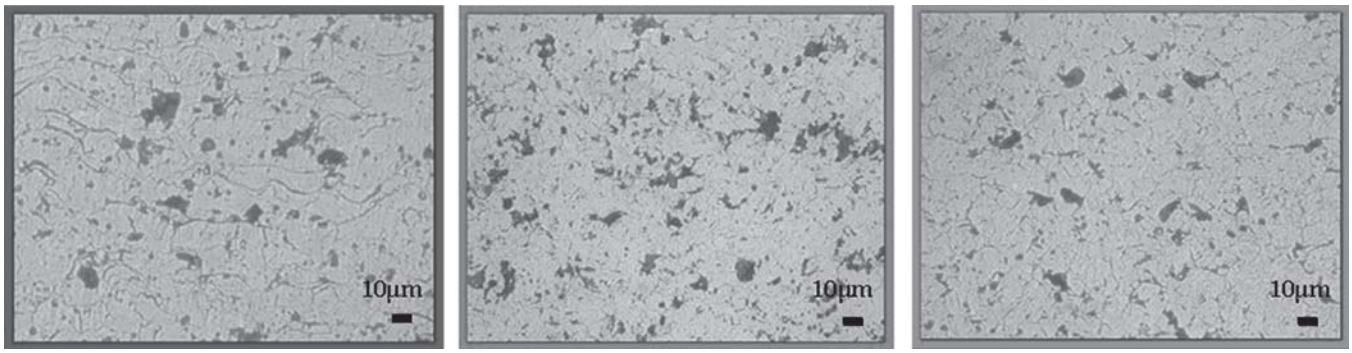

Fig. 2 Images of cross sections of coatings made using different feedstock powders: (a) HOSP; (b) A&S; (c) F&C

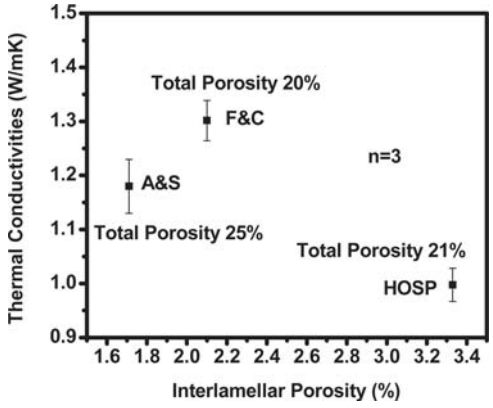

Fig. 3 Relationship between microstructure defects and room-temperature thermal conductivity of YSZ coatings made of different morphology powders

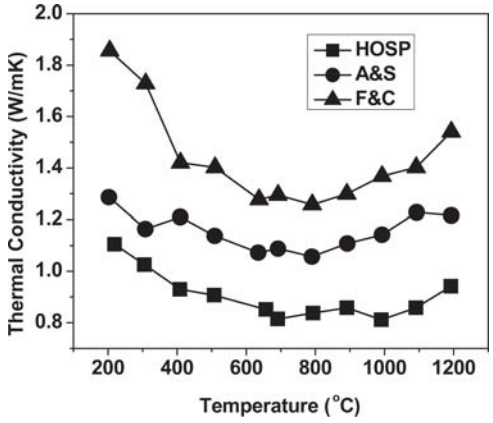

Fig. 4 Temperature dependence of thermal conductivity for YSZ coatings made of different morphology powders

to generate a range temperature and velocity of particles as displaced in the first order process map shown in Fig. 5 (Ref 12). The temperatures and velocities were measured at the maximum flux location of the spray stream using the "Tecnar DPV 2000" (St-Bruno, QC, Canada) (Ref 21). Details of this process map study and its implications on microstructure development are presented elsewhere (Ref 17, 22, 23).

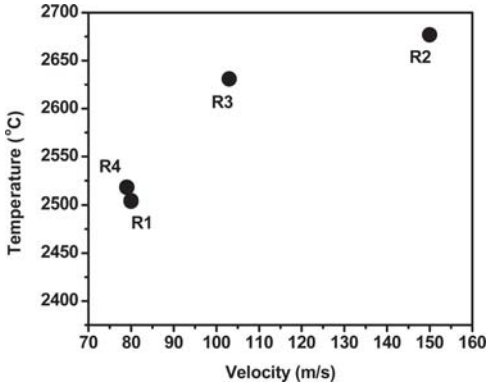

Fig. 5 Process map of YSZ coatings. Temperature (T) and velocity (V)

Figure 6 shows the thermal conductivities and total porosity relationship of YSZ coatings made at different temperature and velocity. Inverse dependence of the experimental results of thermal conductivity is observed with respect to the total porosity. The different setting of temperature and velocity using process map (Fig. 5) achieves a wide variation of total porosity, almost 10%, due to the different melting state and kinetic state and thus the different degree incomplete contact among splats. Higher temperature and velocity result in higher flatting ratio of splats and thus more interfaces per unit thickness. On other hand, they improve the contact between splats and decrease the interlamellar porosity. For the four coatings in Fig. 6, similar interlamellar porosity of around 2% is attained due to the effects of the two aspects. Therefore, the difference of total porosity resulting from diverse particle states plays a dominant role in thermal conductivity variation.

3.3 Anisotropy of Thermal Conductivity for YSZ Coating

The plasma sprayed process involves melting of feedstock materials in a plasma plume and rapidly transporting these molten particles to the substrate, where rapid solidification of individual particle occurs upon impingement. Successive buildup of these "splats" results in a layered arrangement in the coating, analogous to a brick-wall-like structure where the splats are entwined in complex arrays (Ref 24, 25). This splat-based layered microstructure leads to an intrinsic anisotropy of the coating in the direction perpendicular to the spray direction. Thus, micro-

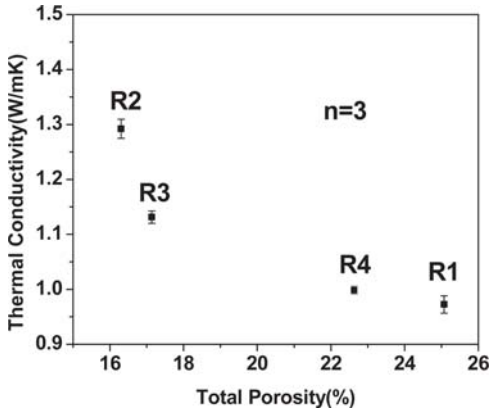

Fig. 6 Correlation between room-temperature thermal conductivities of YSZ coatings and their porosities

structural anisotropy results in anisotropy of coating property. Kulkarni et al. (Ref 2) quantified microstructure (porosity, opening dimension, orientation, and morphology) in plasma sprayed YSZ coatings by means of small-angle neutron scattering and used image-based finite-element analysis to extract thermal conductivities in both through-thickness and in-plane orientations. The results were assembled to explain the anisotropy of coating nature by the orientation of the cracks and interlamellar pores.

In this study, anisotropic thermal conductivity of YSZ coating sprayed with the same T, V was compared. Although the through-thickness thermal conductivities were reasonably accurate and stable, the in-plane measurements presented a larger error. In Fig. 7, all the effective thermal conductivities are slightly higher in plane than through thickness. This trend can be elucidated by the quantity of interlameller pores and vertical cracks as the simulation model (Ref 2). When the amount of interlameller pores is larger than that of vertical cracks, a higher thermal resistance to the heat flux generates in the vertical direction than in the horizontal direction. The difference in the effective thermal conductivities in the two directions is not significant due to the small difference of the quantity of interlameller pores and vertical cracks.

3.4 Comparing Thermal Diffusivity Measurement Methods

Both xenon flash and laser flash were used for thermal diffusivity measurement at room temperature. A comparison is shown in Fig. 8 and 9. For three different morphology YSZ ceramic coatings (Fig. 8), the thermal diffusivities measured by two methods are very close. The laser flash data are marginally higher due to little shorter pulse time and half rise time $t_{1/2}$ of laser than that of xenon (α is inverse to $t_{1/2}$) (Ref 9). This demonstrates the fidelity of the thermal diffusivity measurements for the plasma sprayed YSZ coatings.

Thermal diffusivity measurements were also conducted for plasma sprayed Si and Mo coatings. Figure 9 shows both laser flash and xenon flash results. The results show large discrepancy for Si thermal diffusivity by these techniques, with the xenon flash reporting much lower than that from laser flash. Here the laser flash data is more appropriate to consider for the measured coatings. The time taken for the back surface to reach half its

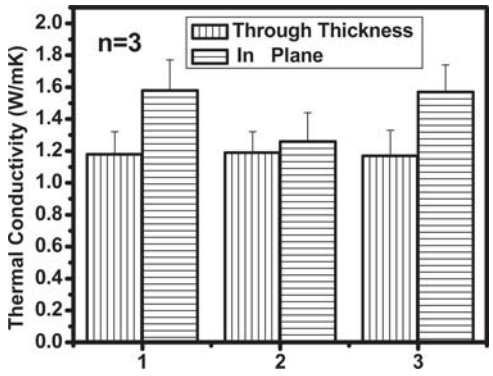

Fig. 7 Room-temperature thermal conductivity of YSZ coatings in different direction

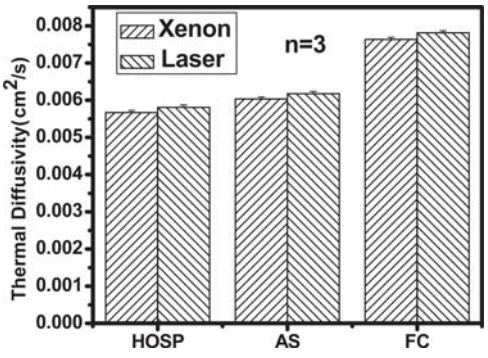

Fig. 8 Thermal diffusivity measurements by xenon and laser flash at room temperature of ceramic coatings

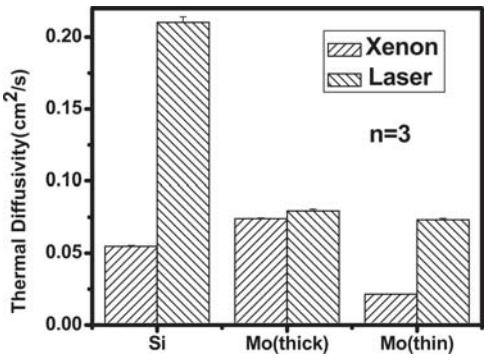

Fig. 9 Thermal diffusivity measurements by xenon and laser flash at room temperature of semiconductor and metal coatings

maximum temperature ($t_{1/2}$) should be at least three times longer than the pulse time. Due to high thermal diffusivity, $t_{1/2}$ of xenon flash is smaller than the optimum range, which causes much bigger error for xenon than laser due to longer pulse time of xenon. For the metal molybdenum coating, two samples are measured (Fig. 9): one is thick (about 1.1 mm) and the other is thin (0.45 mm). For the thick samples, the thermal diffusivities measured by xenon flash and laser flash are similar. However, for the thin sample, the result of laser flash is much higher than that of xenon flash. Again, the $t_{1/2}$ of xenon flash is smaller than the optimum range (three times larger than xenon pulse time) due to too small

thickness and the correction for the finite width of the pulse becomes severe. For metal coatings, this causes the substantial error for xenon flash but not for laser flash due to longer pulse time of xenon.

4. Conclusions

Three techniques were adopted to explore the thermal conductivities of a variety of plasma sprayed coatings. The laser flash instrument operated at room temperature is able to measure both thermal diffusivity and conductivity directly. The ceramic coatings produced with varying feedstock morphologies and varying particle states were investigated via this technique in an effort to establish the relationship between thermal conductivities and microstructural defects. The results point to the important role of interlamellar porosity in both room-temperature and temperature-dependent thermal conductivity. The high-temperature laser flash system at Oak Ridge National Laboratory (ORNL) was used for high-temperature thermal property measurement. The microstructural effects are seen in the high-temperature results as well indicating the strong role of interlamellar porosity on high-temperature thermal barrier effect. The xenon flash method in conjunction with specific heat measurement represents an excellent method for rapid measurement of room-temperature thermal conductivity for ceramic coatings. For the case of metal and semiconductor coatings, the coating thickness must be carefully considered to get accurate information for both techniques. This study clarifies these findings and also provides a pathway to establishing the critical link between process-microstructure and thermal properties of thermal sprayed coatings. The thermal exposure results in the closure of interlamellar pores (Ref 26), which is known to sinter and affects thermal conductivity (Ref 13, 27). A symmetric work involving the sintering effect is underway in an effort to provide quantitative correlation between thermal conductivity and interlamellar porosity.

Acknowledgments

This research was supported by the MRSEC program of the National Science Foundation under award DMR 0080021 and Assistant Secretary for Energy Efficiency and Renewable Energy, Office of Transportation Technologies, as part of the High Temperature Materials Laboratory User Program at Oak Ridge National Lab by the UT-Battelle LLC, for the Department of Energy under contract DE-AC05000OR22725. The authors thank V. Srinivasan, A. Vaidya, and G. Bancke for their help with specimen preparation.

References

1. R.A. Miller, Current Status of Thermal Barrier Coatings, *Surf. Coat. Technol.,* 1987, **30**(1), p 1-11
2. A. Kulkarni, Z. Wang, T. Nakamura, S. Sampath, A. Goland, H. Herman, J. Allen, J. Ilavsky, G. Long, J. Frahm, et al., Comprehensive Microstructural Characterization and Predictive Property Modeling of Plasma Sprayed Zirconia Coatings, *Acta Mater.,* 2003, **51**(9), p 2457-2475
3. D. Zhu and R.A. Miller, Thermal Barrier Coatings for Advanced Gas-Turbine Engines, *Mater. Res. Bull.,* 2000, **25**(7), p 43-47
4. L. Pawlowski and P. Fauchais, Thermal Transport Properties of Thermally Sprayed Coatings, *Int. Mater. Rev.,* 1992, **37**(6), p 271-290
5. K.W. Schlichting, N.P. Padture, and P.G. Klemens, Thermal Conductivity of Dense and Porous Yttria Stabilized Zirconia, *J. Mater. Sci.,* 2001, **36,** p 3003-3010
6. R. McPherson, A Model for the Thermal Conductivity of Plasma Sprayed Ceramic Coatings, *Thin Solid Films,* 1984, **112**(1), p 89-95
7. M.V. Swain, L.F. Johnson, R. Syed, and D.P.H. Hasselman, Thermal Diffusivity, Heat Capacity and Thermal Conductivity of Porous Partially Stabilized Zirconia, *J. Mater. Sci. Lett.,* 1986, **5,** p 799-802
8. R.E. Taylor, Thermal Conductivity Determinations of Thermal Barrier Coatings, *Mater. Sci. Eng. A,* 1998, **245,** p 160-167
9. H. Wang and R.B. Dinwiddie, Development of a LabView™ Based Portable Thermal Diffusivity System, *Thermal Conductivity 27/ Thermal Expansion 15,* H. Wang, Ed., Des Tech Publishing, 2004, p 484-492
10. A. Kulkarni, J. Gutleber, S. Sampath, A. Goland, W.B. Lindquist, H. Herman, A.J. Allen, and B. Dowd, Studies of the Microstructure and Properties of Dense Ceramic Coatings Produced by High-Velocity Oxygen-Fuel Combustion Spraying, *Mater. Sci. Eng. A,* 2004, **369**(1-2), p 124-137
11. H. Wang and R.B. Dinwiddie, Multiple Station Thermal Diffusivity Instrument, *Thermal Conductivity, 23,* K.E. Wilkes, R.B. Dinwiddie, and R. S. Graves, Ed., Technomic Publishing Co., 1996, p 119-127
12. A. Vaidya, "Process Maps for Thermal Spray: A Fundamental Approach to Process-Property Relationships," Ph.D. thesis State University of New York at Stony Brook, 2004, p 183
13. A. Kulkarni, A. Vaidya, A. Goland, S. Sampath, and H. Herman, Processing Effects on Porosity-Property Correlations in Plasma Sprayed Yttria Stabilized Zirconia Coatings, *Mater. Sci. Eng. A,* 2003, **359,** p 100-111
14. S. Sampath, V. Srinivasan, A. Vaidya, A. Gouldstone, Y. Liu, and T. Nakamura, Sensing, Control, and In situ Extraction of Coating Properties: An Integrated Approach towards Establishing Process Maps, *Thermal Spray Conference & Expositions (ITSC)* (Seattle, WA), 2006, Electronic Proceedings
15. A. Vaidya, T. Streibl, S. Sampath, and H. Zhang, A Comparative Diagnostic Analysis of Morphologically Different YSZ Powders, *Thermal Spray Solutions: Advances in Technology and Application (ITSC 2004)* (Osaka, Japan), 2004, ASM Electronic Proceedings
16. M. Friis, C. Persson, Control of Thermal Spray Processes by Means of Process Maps and Process Windows, *J. Therm. Spray. Technol.,* 2003, **12**(1), p 44-52
17. S. Sampath, X. Jiang, A. Kulkarni, J. Matejicek, D.L. Gilmore, and R.A. Neiser, Development of Process Maps for Plasma Spray: Case Study for Molybdenum, *Mater. Sci. Eng. A,* 2003, **348**(1-2), p 54-66
18. N.P. Pasture and P.G. Klemens, Low Thermal Conductivity in Garnets, *J. Am. Ceram. Soc.,* 1997, **80**(4), p 1018-1020
19. M. Friis, P. Nylen, and C. Persson, Investigation of Particle In-Flight Characteristics during Atmospheric Plasma Spraying of Yttria-Stabilized ZrO2: Part 1. Experimental, *J. Therm. Spray. Technol,* 2001, **10**(2), p 301-310
20. S. Sampath and X. Jiang, Splat Formation and Microstructure Development during Plasma Spraying: Deposition Temperature Effects, *Mater. Sci. Eng. A,* 2001, **304-306,** p 144-150
21. A. Vaidya, T. Streibl, L. Li, S. Sampath, O. Kovarik, and R. Greenlaw, An Integrated Study of Thermal Spray Process-Structure-Property Correlations: A Case Study for Plasma Sprayed Molybdenum Coatings, *Mater. Sci. Eng. A,* 2005, **403**(1-2), p 191-204
22. M. Friis, C. Persson, and J. Wigren, Influence of Particle In-Flight Characteristics on the Microstructure of Atmospheric Plasma Sprayed Yttria Stabilized ZrO_2, *Surf. Coat. Technol.,* 2001, **141**(2-3), p 115-127
23. S. Deshpande, A. Kulkarni, S. Sampath, and H. Herman, Application of Image Analysis for Characterization of Porosity in Thermal Spray Coatings and Correlation with Small Angle Neutron Scattering, *Surf. Coat. Technol.,* 2004, **187**(1), p 6-16
24. H. Herman, Plasma Sprayed Coatings, *Sci. Am.,* 1988, **259**(3), p 112-117
25. R. McPherson, The Relationship between the Mechanism of Formation, Microstructure and Properties of Plasma Sprayed Coatings, *Thin Solid Films,* 1981, **83**(3), p 297-310
26. R.W. Trice, S.Y. Jennnifer, J.R. Mawdsley, and K.T. Faber, Effect of Heat Treatment on Phase Stability, Microstructure, and Thermal Conductivity of Plasma-Sprayed YSZ, *J. Mater. Sci.,* **37,** p 2359-2365
27. Z. Wang, A. Kulkarni, S. Deshpande, T. Nakamura, and H. Herman, Effects of Pores and Interfaces on Effective Properties of Plasma Sprayed Zirconia Coatings, *Acta Mater.,* 2003, **51**(18), p 5319-5334